Nanoscale

ROYAL SOCIETY OF CHEMISTRY

PAPER

View Article Online
View Journal | View Issue

Cite this: *Nanoscale*, 2023, **15**, 4570

Field-effect transistor antigen/antibody-TMDs sensors for the detection of COVID-19 samples†

Ruben Canton-Vitoria, *[a,b] Kotaro Sato,[c,d] Yashiro Motooka,[c] Shinya Toyokuni,[c] Zheng Liu [e] and Ryo Kitaura *[a,f]

Received 27th November 2022,
Accepted 6th February 2023

DOI: 10.1039/d2nr06630k

rsc.li/nanoscale

We fabricated sensors by modifying the surface of MoS_2 and WS_2 with COVID-19 antibodies and investigated their characteristics, including stability, reusability, sensitivity, and selectivity. Thiols and disulfanes in antibodies strongly interact with vacant Mo or W sites of MoS_2 or WS_2, yielding durable devices that are stable for several days in the air or water. More importantly, detachment of the antibodies is suppressed even during the aggressive cleaning process of the devices at pH 3, which allows reusing the same device in several experiments without appreciable loss of sensitivity. Therefore, the nanodevice may be employed in samples of different patients. Further, we found a limit of detection (LOD) of 1 fg ml^{-1} at room temperature, time responses of 1 second, and selectivity against interferences such as KLH protein or Albumin.

Introduction

COVID-19 has threatened people worldwide, and there is no end to the news about deaths, infections, and restrictions. The surface of the COVID-19 virion (the entire virus particle) has a protein membrane, two sub-units of spike glycoprotein (S1 and S2), and nucleocapsids. Each virion has approximately 100 spike glycoproteins,[1,2] which can interact with a vasodilator protein, the host cell's angiotensin-converting enzyme 2 (ACE2). COVID-19 RNA particles initiate replication in the cytoplasm by interacting with the host cell. Meanwhile, IgG or IgM antibodies interact with S1–S2 proteins, neutralizing the virion.[3,4] The vaccine, crucial for the suppression of COVID-19, aims to produce antibodies against the glycoproteins of the spike.[5]

In addition to the vaccine, fast detection of COVID-19 has been essential for all governments to end the pandemic. Usually, virion concentration ranges from 10^4 to 10^7 fg ml^{-1} (copies per ml),[6] and in the case of the most contagious patients, it reaches 10^8–10^{11} fg ml^{-1}.[7–10] Nasopharyngeal swab polymerase chain reaction (PCR) and the serological test have been the most demanded techniques to detect COVID-19. Commercial PCR tests are 99% reliable and have a limit of detection (LOD) for RNA SARS-CoV-2 of less than 20 copies per ml. PCR can detect COVID-19 even 50 days after symptoms have stopped,[11] making it the most sensitive method. Despite its sensitivity, PCR is expensive and needs several hours. On the other hand, the antigen test is cheaper and faster (a few minutes). However, the LOD is 1 ng ml^{-1} (10^6 copies per ml), allowing the detection of COVID-19 only when the viral load is relatively high.

COVID-19 detection is useless unless asymptomatic or symptomatically concealed citizens are tested. A minimally invasive method, such as a nasopharyngeal swab, would motivate citizens to be tested. Saliva is a biological fluid containing 30% of biomolecules in blood, which can be used to detect COVID-19 and IgA antibodies.[12] Saliva may provide more accurate results than a nasopharyngeal swab in some situations.[13–16] Since commercial saliva test kits are now available inexpensively, increasing the sensitivity of these kits is the key to successfully controlling COVID-19 infection.

Nanomaterials are excellent candidates for fabricating sensors. For example, 0-dimensional materials, such as gold nanoparticles, can perform colorimetric assays with a lower detection limit of 180 ng ml^{-1} RNA particles (According to the molecular mass, around 10^{13} copies per ml).[17] Another promising nanomaterial is two-dimensional (2D) materials. For example, field-effect transistor (FET) devices with antibodies/graphene show a sensitivity of 1 fg of S protein per ml (around 10 000 copies per ml).[18] 2D semiconductors, such as transition

[a]*Department of Chemistry, Nagoya University, Nagoya, Aichi 464-8602, Japan. E-mail: rcanton@eie.gr*
[b]*Theoretical and Physical Chemistry Institute, National Hellenic Research Foundation, 48 Vassileos Constantinou Avenue, 11635 Athens, Greece. E-mail: rcanton@eie.gr; Tel: +30 210 7273835*
[c]*Department of Pathology and Biological Responses, Nagoya University Graduate School of Medicine, Nagoya, Aichi 466-8550, Japan*
[d]*Department of Oral and Maxillofacial Surgery, Nagoya University Graduate School of Medicine, Nagoya, Aichi 466-8550, Japan*
[e]*Innovative Functional Materials Research Institute, National Institute of Advanced Industrial Science and Technology (AIST), Nagoya, Aichi 463-8560, Japan*
[f]*International Center for Materials Nanoarchitectonics, National Institute for Materials Science, 1-1 Namiki, Tsukuba 305-0044, Japan*
† Electronic supplementary information (ESI) available. See DOI: https://doi.org/10.1039/d2nr06630k

metal dichalcogenides (TMDs), are also candidates for high sensitivity of COVID-19 detection; WSe_2 has been used as a FET-based sensor, showing a detection limit of 25 pg ml^{-1} (2.5×10^8 copies per ml).[19]

Anchoring antibodies on the surface of 2D materials is essential in fabricating 2D-materials-based sensors. For anchoring antibodies, the primary benefit of covalent functionalization is avoiding organic species (or antibody) detachment. Covalent functionalization has been widely studied in graphene,[20] whereas the studies in TMDs are still under development.[21,22] Focusing on TMDs, the best method for functionalizing semiconducting MoS_2 or WS_2 is undoubtedly the addition of organic compounds with sulphur derivatives such as thiol, dithiolanes, or dithiolenes[21,22] because it prevents disruption of the TMDs basal plane. For example, thiols covalently interact with Mo or W metals through the S vacancy on the basal plane of TMDs. We have employed this strategy on phthalocyanine,[23] porphyrins,[24] polymers,[25] quantum dots[26,27] pyrenes,[28] or perylenes.[29] In addition, we previously proved that pyrene[30,31] and Ni-phorphyrin[32] induces electron transfer, leading to gating on FET devices to modify the carrier density of MoS_2 and WS_2. Thus, a simple procedure should be developed to covalently functionalize TMDs with the cysteine (or cystine) of antibodies. In any manipulation of the further FET device, the strong covalent bound between antibodies and TMDs may impede the separation of both species and must be more beneficial than simple van der Waals forces.

Currently, all the FET nanodevices that detect COVID-19 are extremely sensitive. Previous studies that focused on detecting COVID-19 are based on adding a specific antigen to a single original solution. In terms of reusability, investigations in which the device can easily switch from one solution to another are attractive since they will allow researchers to test samples from various patients using the same device. In this work, we study the capabilities of MoS_2 and WS_2 sensors covalently functionalized with COVID-19 antibodies. The new sensors are made of semiconducting 2-dimensional materials; these characteristics are essential for high sensitivity. The main objective of this contribution was to maximize the stability and interactions between TMDs and antibodies. We employ the chemical properties of the TMDs to have stable covalent functionalization, which allows for cleaning and reusing the devices several times. This condition enables profound studies without the risk of antibody detachment on the device. In addition, the S2 glycoprotein (antigen) on the surface of TMDs-antibodies acts as a gating, producing a robust variation of the conductivity in response to the antigen concentration. The best devices archive a limit of detection of 1 fg ml^{-1} and a time response lower than 1 second. The new material resists common antigen/antibody excision conditions and remains stable after several days stored in the air. Equally importantly, the FET devices show selectivity against interferences such as Albumin or KLH. Furthermore, we demonstrate that the device detects different antigen concentrations in saliva.

Experimental section

We purchased the polyclonal IgG antibodies from rats (SARS-CoV-2 (2019-nCoV) spike S2 antibody) and the commercially available SARS-CoV-2 (2019-nCoV) spike S2 ECV-His recombinant protein (antigen) that are derived from the original form COVID-19. The structures of a representative antibody[33,34] and S2 protein (antigen) are shown in Fig. S1.†

Substrate treatment

SiO_2/Si substrates 6×2 cm^2 were washed in piranha solution for 15 minutes under sonication, followed by 1 minute of sonication in ultrapure H_2O and MeOH. After the sonication, substrates were dried using N_2 blowing, and then the substrates were heated at 700 °C under an airflow of 400 ml min^{-1} for 30 minutes.

Example of chemical vapor deposition (CVD) synthesis of MoS_2 (or WS_2)

15 mg of MoO_3 (or WS_2) containing 15% of NaCl was deposited in the center of an alumina boat (10×1.5 cm^2) with a height of 1.1 cm. The boats were put in a quartz tube (3 cm in diameter). MoO_3 was gradually heated up to 725 °C (780 °C) in 13 minutes with an Argon flow rate of 113 ml min^{-1}. Then, Sulphur was also heated up to 210 °C for 10 minutes. All CVD parameters were kept constant during 5–10 additional minutes before cooling down. The step of cooling down (from 700 to 300 °C) was very slow (several hours) to abolish the partial metallic phase.[35,36]

Covalent functionalization between antibody and MoS_2

5 μl of 100 μg ml^{-1} of antibody in water was deposited on a substrate with pristine MoS_2. The substrate was put in a box of $2 \times 2 \times 1$ cm^2 to avoid vaporization of water and kept at 4 °C for 10 days. After this process, water was removed by drying the substrate on a hot plate at 40 °C for 10 min. Finally, weakly attached antibodies (non-covalent) were removed by washing with pure water in 10 different vials. After the second wash, grids of ELISA test provide negative value towards Ellman's reagent, suggesting an absence of a detachment of antibodies from the antibody-MoS_2 device.

Covalent functionalization between cysteine and MoS_2

We performed the reaction towards exfoliated and CVD-TMDs on SiO_2 substrate with electrodes. MoS_2 was immersed in 5 ml of Dimetilacetamide (DMAc) with the maximum amount of cysteine dissolved. We kept the reaction for four days in N_2 at 50 °C under a dark environment. Then, it was cleaned with pure DMAc four times by immersion. Later, non-covalent species were entirely removed by using carbon sulfide under Solhex reflux for 12 h. Finally, the device was washed once more with water. The water used for cleaning was tested by Ellman's reagent. A negative value suggests the absence of a detachment of antibodies from the antibody/MoS_2 device.

Coulombic interactions between antibody cysteine-MoS_2 (antigen-cysteine-MoS_2)

5 μl of 100 μg ml^{-1} of antibody in water was deposited on a substrate with pristine CVD MoS_2. The substrate was covered in a box of 2 × 2 × 1 cm^2 and kept at 4 °C for 1 day. The box forbids the evaporation of water. After this period, the substrate was immersed several times in water to detach antibodies that were weakly attached to the surface.

Device fabrication

Firstly photoresist (ZEP520A) was spin-coated (1000 rpm 5 s and 6000 rpm 50 s) onto pristine CVD-MoS_2 (or WS_2) on SiO_2 270 nm/Si. And then, we heated it for 2 minutes at 180 °C in the air and put it in the EBL chamber for the electrode patterning. AutoCAD2020 and Wecas were employed to design electrode patterns. We used 20 kV acceleration voltage and 5 nA current to draw the electrode patterns in the EBL. The developing process was performed by immersing substrates into *o*-xylene for 10 seconds. Metal depositions of 10 nm of Cr and 50–80 nm of Au were carried out with a vacuum deposition chamber working at 10^{-7} Torr. The process was repeated with 10 nm of Bi and 50 nm of gold, ensuring direct contact between Bi/Au and the channel. Note that Cr provides mechanical resistance to the device, and Bi reduces the Schottky barrier for low contact resistance. During the deposition, substrates were kept cold at 10 °C using a water cooler system. The lift-off process has been performed with DMAc at room temperature. The devices were heated at 250 °C under Ar/H_2 flow of 400/30 ml min^{-1} to increase the conductivity. After covering the electrodes with ZEP520A, we added the antibodies. After the covalent functionalization, we covered the whole substrate surface (but not the area of TMDs) with PPC. In total, we successfully performed 14 devices to study the properties of antibody-TMDs: 1 device of antibody-WS_2, 1 device for MoS_2 functionalized with cysteine to study its properties, 6 additional devices of antibody-MoS_2 to study the interaction with interferences, 2 devices for saliva studies, 2 blank experiments and 2 for study the stability of the devices.

Evaluation of sensors

All the experiments were carried out at 25 °C under dark conditions. The gate and vias voltages were set to 0 and 0.5 V, respectively. The devices were immersed in 96-ELISA grids (no ELISA test) with antigens at different concentrations. The solution inside the grid was mechanically homogenized by immersing and removing the device three times. Before changing to another ELISA grid with a crescent antigen concentration, the device was washed with HCl/glycine buffer at pH = 3 by five consecutive immersions for 10 seconds. Then, the pH was recovered by five additional immersions in different ELISA grids with ultrapure water. Check a representative example in Scheme S1 at ESI.†

Additional information about characterizations, including AFM, TEM, and Raman, are shown in the supplementary Experimental section in the ESI.†

Results and discussion

To begin with, Fig. 1a shows the complete fabrication process of COVID-19 sensors. According to our previous work, the semiconductor channel (MoS_2 and WS_2) of the device for detecting COVID-19 was grown with the chemical vapor deposition method.[35,36] First, interdigitated electrode patterns were deposited on the MoS_2 or WS_2 channel (10 Cr/Au 60 nm and Bi 20 nm/Au 60)[36] and then non-conductive polymers were put outside of the channel to insulate the electrodes. Afterward, we carried out the functionalization of TMDs with antibodies.

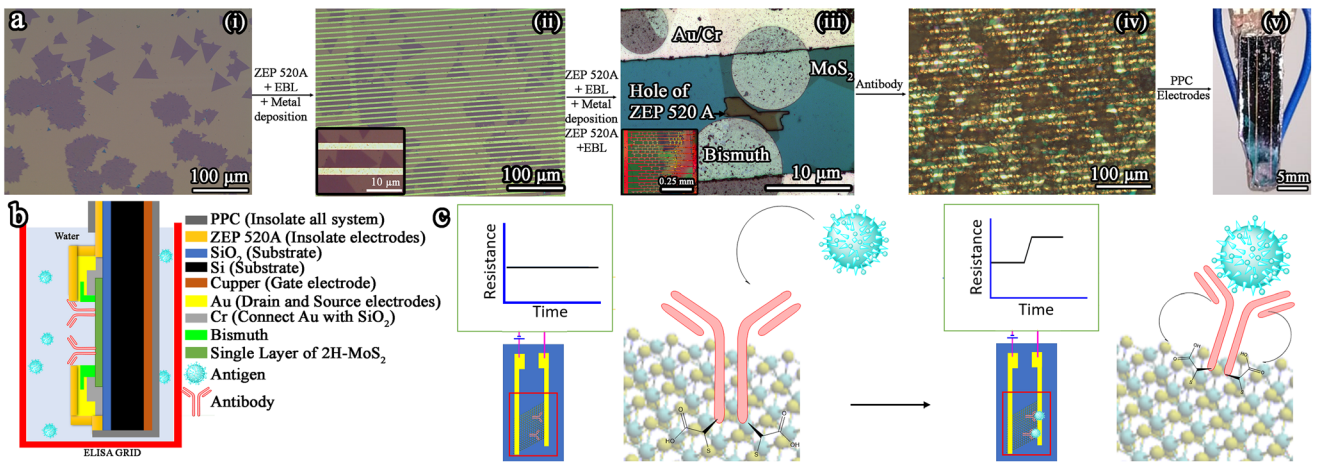

Fig. 1 (a) Optical pictures showing the fabrication procedure of antibody-MoS_2 sensors. (i) CVD-MoS_2 taken with a low magnification, (ii) a device with gold electrodes at 5 and inset; 50 magnifications. (iii) FET MoS_2 device with Gold and Bismuth electrodes covered with ZEP 520 A insulate polymer at 50 and inset; 5 magnifications. (iv) Antibody-MoS_2 device at 5 magnifications. (v) Antibody-MoS_2 device connected to the Keithley semiconductor parameter analyzer. (b) Representative FET Antibody-MoS_2 device. (c) Model: response mechanism of antibody-MoS_2 without (left) and with (right) antigen.

Due to the low thermal stability of the antibodies, we performed the reaction at 4 °C for 10 days (see Experimental section). Basically, the thiols in our antibodies (calculate as 3% of cysteines in weight by *Ellman's reagent vs.* 1% in antigens)[34,37] react with bare metals at sulphur vacancies of MoS_2 and WS_2.[21–33] Maldi-fingerprint before and after the reaction are identical, showing that antibodies do not degrade after the reaction (see ESI Fig. S2a†). After extensive washing, all the non-covalent antibodies were removed from the device. It should be noted that such washing damages non-covalently functionalized single-layer MoS_2 because the surface tension of water breaks the single-layer MoS_2. In contrast, antibodies on MoS_2 act as a surfactant, stabilizing the device (see ESI Fig. S2b†). Indeed, devices incubated with antibodies for 1 or 4 days were destroyed, while the device with 10 days of incubation resisted the water-cleaning process. The final 250 μl of water used to wash the device revealed neither thiols nor amines by *Ellman's reagent* or *Kaiser* test. The device, therefore, is free of non-covalent species and stable in solvents with high surface tension. Deposition of antibodies on MoS_2 with shorter times (overnight) shows a complete detachment of the antibodies, suggesting that thiols need time to have strong interactions with the surface of MoS_2. It is unknown if earlier TMD-based devices were covalently or non-covalently functionalized with anibodies,[19] but the experiment described in the bibliography does not fully employ the capabilities of covalent functionalization. The main advantages of our methodology include higher reusability, durability, and, importantly, the ability to switch the device from one solution to another. Fig. 1b shows a schematic drawing of the device, in which only antibody-MoS_2 can directly contact the antigen, insulating other components such as electrodes. Once the antigens interact with antibodies, the antigen–antibody complexes should modify the electronic properties of antibodies, which leads to a change in the electronic density at the surface of MoS_2. In other words, antibodies that bind to antigens operate as a gate voltage, inducing a change in the carrier density of the device (see the model in Fig. 1c).[19,38,39]

We performed structural characterization using a transmission electron microscope (TEM) and an atomic force microscope (AFM). Concretely, AFM observations revealed that the height variation caused by the antibodies typically increases by about 100 nm. TEM inspection confirmed that CVD-grown samples have sulphur vacancies that can interact with antibodies. The spectroscopic analysis also provided relevant information regarding covalent functionalization. For example, amines or aliphatic chains of antibodies were observed in Raman spectra. More importantly, the intensities of 2LA(M) of MoS_2 bands decrease after functionalization, which is associated with covalent functionalization.[21–25,28–33] Further, XPS suggests reducing the number of sulphur defects, in agreement with Raman.[28,30] Finally, we could not detach the antibodies from MoS_2 without breaking the devices. A brief description of AFM, TEM, and Raman was included in ESI and Fig. S3–S5.†

Next, devices based on MoS_2 were fully optimized. Regarding electrodes, Bi/Au increased the conductivity[36,40] while Cr/Au improved the mechanical resistance. The annealing process (H_2/Ar at 250 °C) results slightly beneficial, increasing the conductivity of the system by 30%. Further, the devices should not have a voltage drain to source (V_{ds}) larger than 0.6 V in water to avoid any unwanted reaction such as hydrogen evolution reaction (HER),[27] or oxygen reduction reaction (ORR);[41] in fact, we observed bubbles and white precipitates form under large V_{ds}. On the other hand, our devices have on/off ratios of 10^8 in the air (see Fig. S6†) due to the semiconducting character of MoS_2. In addition, the threshold voltage (V_{th}) tends to be near to 0 V_G in pristine MoS_2 or antibody-MoS_2 FET devices (see Fig. 2a). In opposite, when the antigen interact with antibody-MoS_2 the charge distribution of the antibodies are modified altering the surface of the MoS_2.[19,38,39] Such electronic changes strongly modify the output characteristics and transfer curves of antibody-TMDs devices (see Fig. S7† and the model shown in Fig. 1c).

Antibodies usually interact with antigens strongly, making the cleaning process very difficult. We found that using HCl/Glycine buffer at pH = 3 modified the tertiary/quaternary structure of the antibody, allowing easy separation of the antigen.[42–45] Blank experiment in Fig. S8† suggests that HCl/Glycine does not damage the antibodies, and the conductivity is easily recovered (See Fig. S8†). Under such conditions, the antibodies were not detached from the surface of MoS_2 due to the covalent character of the hybrid antibody/MoS_2, as a considerable advantage compared with the previous studies based on non-covalent functionalization nanodevices for the detection of COVID-19. The substantial increase of conductivity during washing agrees with the adsorption of positive charges on the antibody and, consequently, in the surface of MoS_2 (see Fig. 2b). As seen in Fig. 2b, the conductivity under a pH of 7 recovers the baseline level during the water washings. Such a procedure can be used typically 15 times before a device gets partially damaged.

Fig. 2c shows a continuous decrease of the conductivity at increasing concentrations of antigen measured with a 96-grids ELISA plate (do not confuse with ELISA test). To improve visualization, we normalize the baseline (Q Water) to 100 A and remove the response variations caused by the cleaning procedure. Similarly, Fig. 2d shows a continuous variation of the response (C_q) under increasing antigen concentrations (C_e). The detection limit was 4.8 pg ml^{-1}, and the response decreased to 6.2 ng. Based on the molecular weight of **1**- the antigen, **2**- the virion (each virion has a mass of ≈1 fg)[6,46] and **3**- the average of S2 glycoprotein in a virion, (~100 units)[1,2] we barely estimated that the LOD 4.8 pg ml^{-1} would correspond to ~48 M of copies per ml. The devices of pristine MoS_2 (blank experiments) showed a maximum sensitivity of 16 000 ng ml^{-1} for S_2 glycoprotein. Moreover, the attachment of antibodies increases the sensitivity in 32 000-fold. In addition, pristine MoS_2 devices (blank experiments) enhance the conductivity of the device, in sharp contrast with antibody-MoS_2 devices, probably because the antigen acts merely as electrolyte in blank experiment (see Fig. S.8†). Fig. 2e shows the Langmuir plot of antibody-MoS_2 device resulting in a perfect linear fitting. This

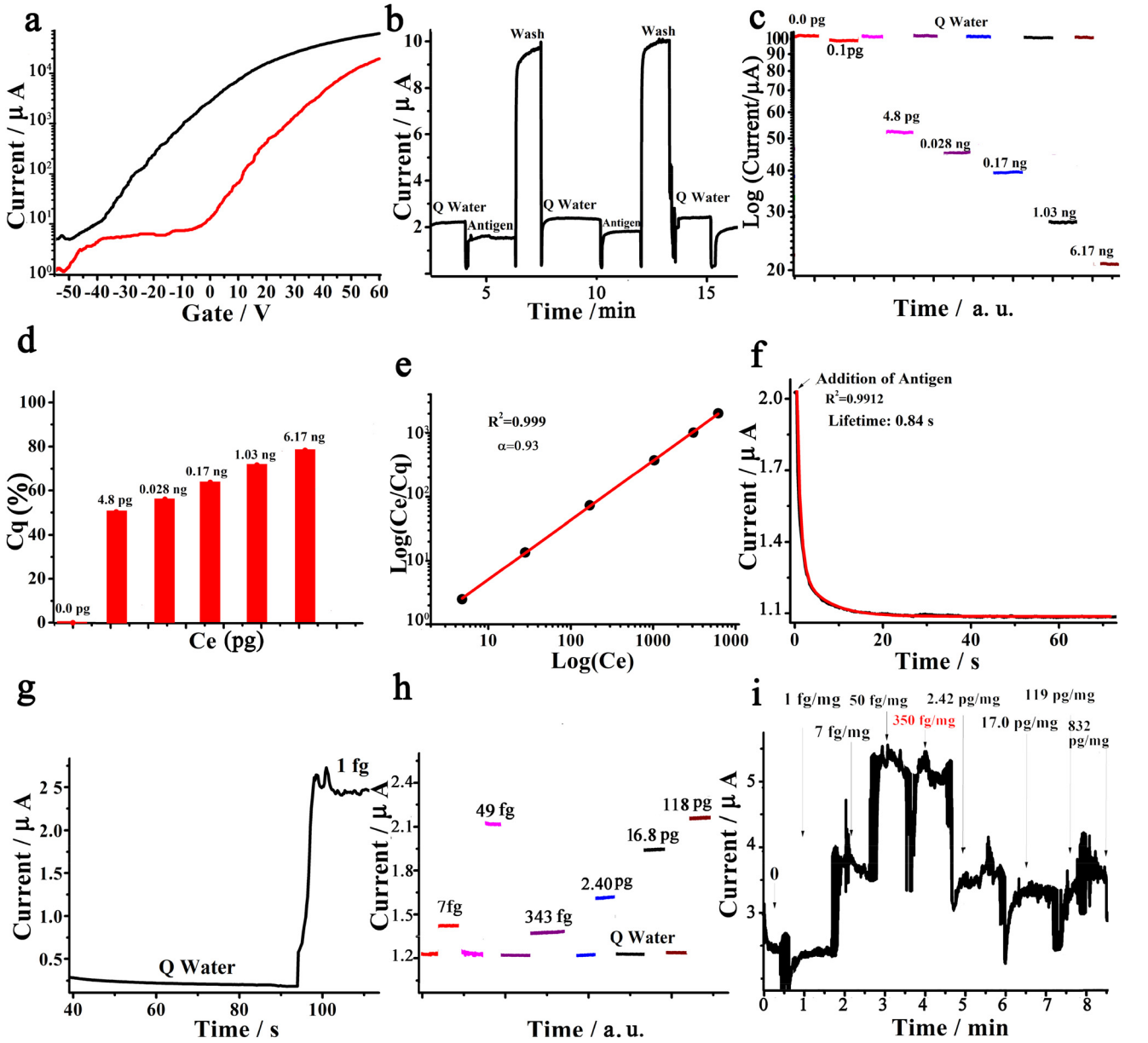

Fig. 2 (a) Transfer curve of (black) MoS_2 and (red) Antibody-MoS_2. Response of FET Antibody-MoS_2 device at (b) constant and (c and d) increasing antigen concentration. (e) Evaluation of concentration and response following logarithmic scale of Langmuir equation (f) Time response of a FET Antibody-MoS_2 interacting with the antigen. (g) First addition and (h) additional additions of antigen to FET Antibody-WS_2 device in water. (i) Response of FET device based on Coulomb interactions of Antibody and MoS_2 in water, at increasing concentrations of antigen. All the experiments were carried out at $0.5V_{D-S}$.

indicates that antibodies on the surface of the device work as strong binding sites for S2 glycoproteins. The plot $[(C_e/C_q = 1/(Q \times q_{max} \times K_L) + C_e/(Q \times q_{max})]$ is usually employed to get more specific information about the antigen–antibody complex.[47] Herein, K_L is the constant related to the affinity of the binding sites (obtaining a value of: 0.002 ml pg^{-1}), q_{max} is the maximum absorption capacity and Q is the constant that connects the variation of current with Langmuir equation. Although the final two factors cannot be calculated independently, $Q \times q_{max}$ offers a value of 446 000 nA mg g^{-1} and may be used to compare to other analytes such as interferences (see below). Since Langmuir plot has R^2 = 0.999, the model perfectly matches with our results, indicating that antibodies are not detached during the measurement. Therefore, additional interpretation with Freundlich or Temkin models are unnecessary. Beyond the sensitivity, a fast response is strongly demanded in biosensing. Fig. 2f shows a time-response of the sensor, which can be fitted by a mono-exponential function with a time-response of 0.8 ± 0.3 s. The recovery time, on the other hand, was 2 ± 0.5 s. These values are

comparable to other FET devices, typically ranging between 5 s ~ 1 min (ref. 48) (see Table 1).

In contrast with antibody-MoS_2, devices based in antibody-WS_2 increases conductivity. The best LOD for antibody-WS_2 devices was 1 fg ml^{-1}, estimated in around 10.000 copies of virion per ml (see Fig. 2g and h). Such detection limit is low enough to be used in infected patients wherein the average of virions copies per ml is 10^4–10^7 (~10^6–10^9 S2 glycoproteins). However, the stability of WS_2 devices was worse than MoS_2. For instance, the response decreases after 7 and 343 fg additions, suggesting that some single layers of WS_2 degrade during the cleaning process, invalidating accurate experiments such as Langmuir plots at the full range of the experiment. The low stability of WS_2 can be associated with a wide range of factors. WS_2 crystals probably grow faster than MoS_2 crystals during CVD synthesis, resulting in more defective material with worse mechanical properties. However, the logarithm of the Langmuir plot displays R^2 of 0.999 for a range of 343 to 118 000 fg ml^{-1}, where some layers of WS_2 are still stable. Moreover, the device allows to calculate the K_L and $Q \times q_{max}$ of the Langmuir plots with relative precision, obtaining values of 1.77 ml pg^{-1} and 2200 nA pg g^{-1}, respectively. The value of $Q \times q_{max}$ does not provide relevant information when antibody-MoS_2 and antibody-WS_2 are compared, since Q depends on each device, but a higher value of K_L in WS_2 device agrees with and improvement of the LOD.

We also fabricated another type of device through the following couple of steps: **1**- we perform the covalent functionalization on the surface of MoS_2 with cysteine. **2**- we add antibodies (see Experimental section). In this sensor (antigen-cysteine-MoS_2), the antibodies interact with cysteine through Coulomb interaction. Concretely, the carboxylate and ammonium charges of cysteine interacts with the charged amino-acids on antibodies (Glutamic acid, Glycine, Leucine or Serine).[27,49] In this case, since the charges of antibodies are closer to the surface of MoS_2 than in cobalent functionalization, we can expect a substantial response against antigen. We remind to the lector that the effect of the charges will decrease with the square of the distance, moreover small distance differences between the charges of antibodies and TMDs in covalent or non-covalent functionalization devices can produce important changes in the conductivity. Due to the weak non-covalent functionalization between cysteine and antibodies, the device was broken after two tests, in the absence of HCl/Glycine or water washing (Fig. 2f). This lack of stability is a proof that the covalent functionalization is effective and necessary to abolish detaching of antibodies in order to reuse devices of TMDs. We try to apply a Langmuir equation between 1–350 fg, obtaining an R^2 = 0.992 which is worse than covalent functionalization but acceptable. Furthermore, the small number of values precludes totally trustworthy values. However, we would like to mention that K_L and $Q \times q_{max}$ are 12 800 ml pg^{-1} and 5060 nA pg g^{-1}, respectively. The huge value of K_L may indicate a close communication between MoS_2 and antibodies. The main advantage of the coulombic interaction methodology is that the detection limit was 7 fg ml^{-1} (70 000 copies), 10^6 better than those of devices fabricated through direct covalent functionalization (see Fig. 2i). In any case, the detection limits that we achieved with any device are much impressive than the best results with the same antibodies reported in other studies, 10 ng ml^{-1}(ref. 50) and comparable with other nanomaterials. Please see Table 1 to easily compare the LOD and lifetime of our devices with some representative examples of the bibliography.

The durability and selectivity of antibody-MoS_2 were also investigated. We employed MoS_2-based devices because of their robustness and high durability. For example, MoS_2-based devices can continuously work for a couple of days in water or more than a week in the air. For example, after 15 days, the response of the device against S2 glycoprotein-antigen barely decreased by 1.5% (see Fig. S9†). Devices based on pristine MoS_2 can interact with electrolytes such as NaCl, modifying the conductivity.[51] In fact, pristine MoS_2 devices start to respond to NaCl at concentrations of 0.23 μg ml^{-1} in pristine MoS_2. On the other hand, the addition of antibodies reduces the sensitivity until 2 mg ml^{-1} (see Fig. S10†). The same device has a maximum response for S2 glycoprotein of 16 000 ng ml^{-1} and 4.8 pg ml^{-1} previous and after functionalization (Fig. 2c *vs.* S8†). Furthermore, the addition of antibodies improves sensitivity to COVID-19 antigens and lowers the sensitivity to other interferences. This phenomenon is easy to rationalize. The antibody insulates the surface of MoS_2, and only those species that strongly interact with antibodies will magnify the response of the device. Fig. 3a and b show that the devices of antibody-MoS_2

Table 1 Comparison of FET antibody-TMDs devices with other representative COVID-19 sensors

Material/device	LOD	Lifetime	Ref.
FET covalent antibody-MoS_2	4.8 pg mL^{-1}	1 s	This work
FET non-covalent antibody-MoS_2	7 fg mL^{-1}	1 s	This work
FET covalent antibody-WS_2	1 fg mL^{-1}	2 s	This work
Colorimetric based sensor with gold nanoparticles	180 ng mL^{-1}	10 min	17
FET non-covalent antibody-graphene	1 fg mL^{-1}	Several seconds	18
FET antibody-WSe_2	25 pg mL^{-1}	2 min	19
FET non-covalent antibody-single wallet carbon nanotube	4.2 fg mL^{-1}	Few seconds	48
Antibodies used in this study employed in ELISA test	50 ng mL^{-1}	No data	50
FET antibody Pt-graphene oxide	1 fg mL^{-1}	Few seconds	52
Colorimetric sensor, antibody-gold nanoparticles	62.5 ng mL^{-1}	1800 s	53 and 54
Resistive sensor of Cys-gold nanoparticles with graphite	229 fg mL^{-1}	6.5 min	55

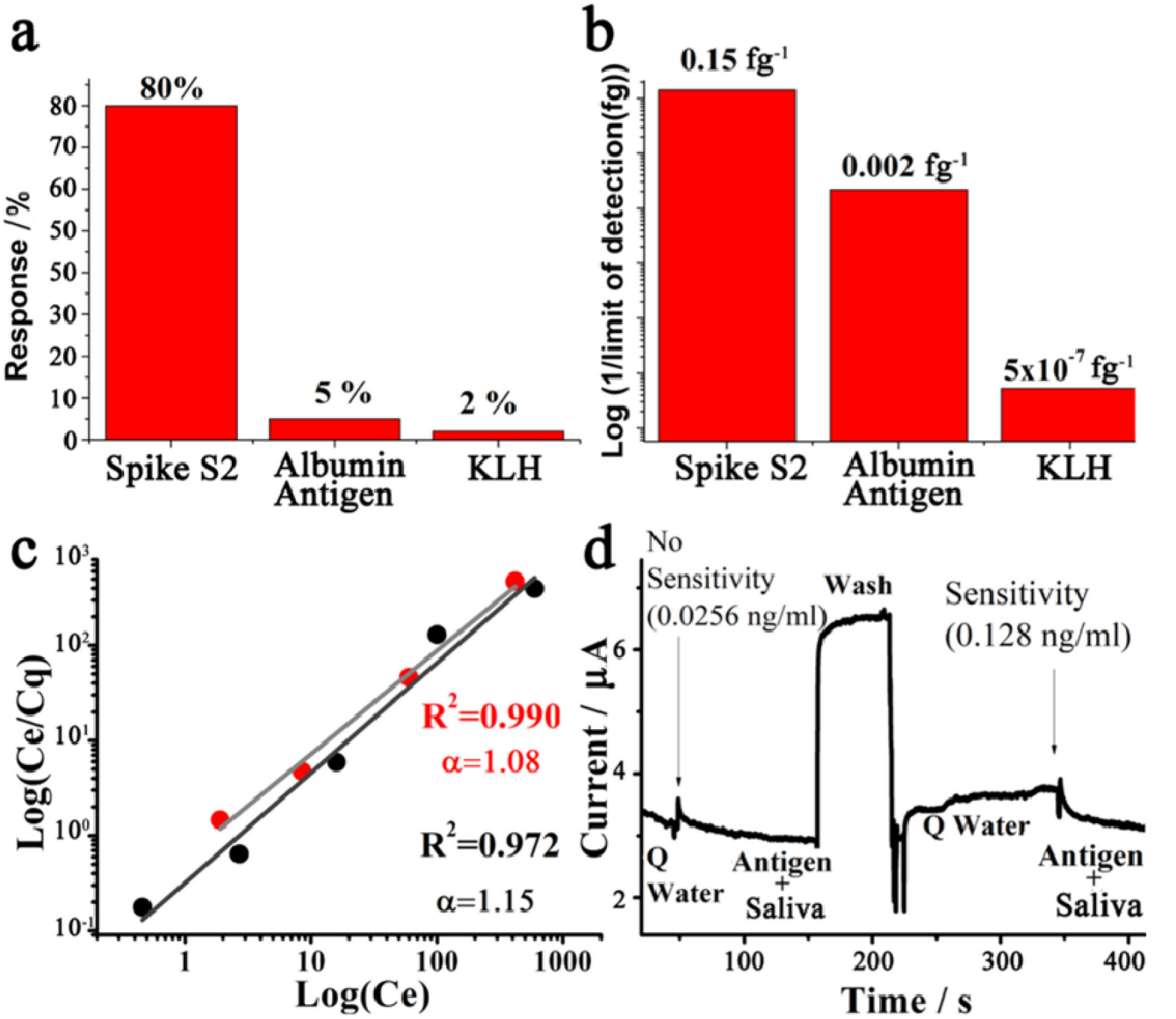

Fig. 3 (a) Response and (b) limit of detection of Albumin and KLH– (c) Logarithmic scale of Langmuir equation for Albumin (red) and KLH (black). (d) Response of FET Antibody-MoS_2 device at increasing antigen concentration in saliva.

barely interact with Keyhole limpet hemocyanin (KLH) protein; the maximum response was 2.0 ± 0.3% at concentrations higher than 2 ng (Fig. S11a†). Fig. 3a and b also show that devices detect Albumin with a concentration of 0.5 ng (Fig. S11b†). The negative charges of Albumin are probably the main reason for the response at low concentrations since the conductivity of n-type MoS_2 should decrease in the presence of negative charges. Such sensitivity to Albumin could interfere with COVID-19 detections. However, the maximum response of Albumin quickly saturates with a 5.0 ± 2.0% variation in the conductivity, whereas a variation of 80 ± 2.0% was observed in the COVID-19 antigen. Fig. 3c shows that Albumin and KLH also follow the Langmuir equation ranging from 0.075 to 595 pg ml^{-1} and 0.29 to 416 ng ml^{-1}, respectively. Finally, the K_L of Albumin and KLH are 23 600 and 3 000 000 smaller than S2 glycoprotein protein. Therefore, we find a strategy to differentiate COVID-19 antigen and potential interferences.

Finally, we tested the effect of saliva (30%) with different antigen concentrations and cleaning the device with HCl/Glycine. Under these conditions, we quickly detected the antigen with a concentration of 128 pg ml^{-1} (1300 M copies) (see Fig. 3d and Fig. S12†). It should be noted that this result is 5-fold better than those studies with the same antibodies/antigen performed by other techniques, such as traditional ELISA assays (ref. 50).

Conclusions

In this work, we have fabricated antibody-TMD devices to detect COVID-19 based on thiol functionalization. The princi-

pal advantage of this study is that antibody-MoS_2 devices allow the measurement of various samples using the same device. Anitibody-MoS_2 devices were stable after several immersion/extraction processes in different antigen, acidic media, or saliva solutions. We found that antibody-MoS_2 has a detection limit of 4.8 pg ml^{-1}. Antigen-WS_2 devices increase the limit of detection to 7 fg ml^{-1}. Next, MoS_2 devices functionalized with cysteine and followed by the addition of antibodies show a significant increase in sensitivity, increasing from 4.8 pg ml^{-1} to 1 fg ml^{-1} since the most charged areas of the antibodies are close to the surface of TMDs. However, detachment of antibodies during cleaning only allows a couple of uses in both antigen-WS_2 and antigen-cysteine-MoS_2, resulting in less interest than antigen-MoS_2. All the devices exhibit a response time of a few seconds and can work even with saliva. The next stage will have to find a strategy that allows connecting the most charged parts of the antibodies directly on the surface of TMDs towards covalent functionalization. This strategy promises to enhance the response and improve the limit of detection while it can be reusable several times. This study has revealed the excellent properties and limitations of TMDs in bionanotechnology.

Conflicts of interest

There are no conflicts to declare.

Acknowledgements

This work was supported by JSPS KAKENHI Grant Numbers JP21K18930, JP20H02566, JP22H05458, JP20H05664, 19F19368, JST CREST Grant Number JPMJCR16F3 and JPMJCR19H4, and JST PRESTO Grant Number JPMJPR20A2. Finally, we thank Kaori Asai for her proofreading.

References

1 B. Turoňová, M. Sikora, C. Schürmann, W. Hagen, S. Welsch, F. Blanc, S. von Bülow, M. Gecht, K. Bagola, C. Hörner, G. van Zandbergen, J. Landry, N. de Azevedo, S. Mosalaganti, A. Schwarz, R. Covino, M. Mühlebach, G. Hummer, J. Krijnse and L. M. Beck, In situ structural analysis of SARS-CoV-2 spike reveals flexibility mediated by three hinges, *Science*, 2020, **370**, 203, DOI: **10.1126/science.abd5223**.

2 H. Yao, Y. Song, Y. Chen, N. Wu, J. Xu, C. Sun, J. Zhang, T. Weng, Z. Zhang and Z. Wu, Molecular Architecture of the SARS-CoV-2 Virus, *Cell*, 2020, **183**, 730, DOI: **10.1016/j.cell.2020.09.018**.

3 L. Mousavizadeh and S. Ghasemi, Genotype and phenotype of COVID-19: Their roles in pathogenesis, *J. Microbiol., Immunol. Infect.*, 2021, **54**, 159, DOI: **10.1016/j.jmii.2020.03.022**.

4 Y. Pan, X. Li, G. Yang, J. Fan, Y. Tang, J. Zhao, X. Long, S. Guo, Z. Zhao, Y. Liu, H. Hu, H. Xue and Y. Li, Serological immunochromatographic approach in diagnosis with SARS-CoV-2 infected COVID-19 patients, *J. Infect.*, 2020, **81**, e28, DOI: **10.1016/j.jinf.2020.03.051**.

5 L. Du, Y. He, Y. Zhou, S. Liu, B. Zheng and S. Jiang, The spike protein of SARS-CoV- a target for vaccine and therapeutic development, *Nat. Rev. Microbiol.*, 2009, **7**, 226, DOI: **10.1038/nrmicro2090**.

6 R. Sender, Y. Bar-On, S. Gleizer, B. Bernshtein, A. Flamholz, R. Phillips and R. Milo, The total number and mass of SARS-CoV-2 virions, *Proc. Natl. Acad. Sci. U. S. A.*, 2021, **118**, e2024815118, DOI: **10.1073/pnas.2024815118**.

7 H. Kawasuji, Y. Takegoshi, M. Kaneda, A. Ueno, Y. Miyajima, K. Kawago, Y. Fukui, Y. Yoshida, M. Kimura, H. Yamada, I. Sakamaki, H. Tani, Y. Moringa and Y. Yamamoto, Transmissibility of COVID-19 depends on the viral load around onset in adult and symptomatic patients, *PLoS One*, 2020, **15**, e0243597, DOI: **10.1371/journal.pone.0243597**.

8 L. Zou, F. Ruan, M. Huang, L. Liang, H. Huang, Z. Hong, J. Yu, M. Kang, Y. Song, J. Xia, Q. Guo, T. Song, J. He, H.-L. Yen, M. Peiris and J. Wu, SARS-CoV-2 Viral Load in Upper Respiratory Specimens of Infected Patients, *N. Engl. J. Med.*, 2020, **382**, 1177, DOI: **10.1056/NEJMc2001737**.

9 K. Walsh, K. Jordan, B. Clyne, D. Rohde, L. Drummond, P. Byrne, S. Ahern, P. Carty, K. O'Brien, E. O'Murchu, M. o'Neill, S. M. Smith, M. Ryan and P. Harrington, SARS-CoV-2 detection, viral load and infectivity over the course of an infection, *J. Infect.*, 2020, **81**, 357, DOI: **10.1016/j.jinf.2020.06.067**.

10 W. Wang, Y. Xu, R. Gao, R. Lu, K. Han, G. Wu and W. Tan, Detection of SARS-CoV-2 in Different Types of Clinical Specimens, *J. Am. Med. Assoc.*, 2020, **323**, 1843, DOI: **10.1001/jama.2020.3786**.

11 Z. Yongchen, H. Shen, X. Wang, X. Shi, Y. Li, J. Yan, Y. Chen and B. Gu, Different longitudinal patterns of nucleic acid and serology testing results based on disease severity of COVID-19 patients, *Emerging Microbes Infect.*, 2020, **9**, 833, DOI: **10.1080/22221751.2020.1756699**.

12 N. Pisanic, P. Randad, K. Kruczynski, Y. Manabe, D. Thomas, A. Pekosz, S. Klein, M. Betenbaugh, W. Clarke, O. Laeyendecker, P. P. Caturegli, H. B. Larman, B. Detrick, J. K. Fairley, A. C. Sherman, N. Rouphael, S. Edupuganti, D. A. Granger, S. W. Granger, M. H. Collins and C. D. Heaney, COVID-19 Serology at population scale: SARS-CoV-2-Specific antibody responses in saliva, *J. Clin. Microbiol.*, 2020, **59**, e02204, DOI: **10.1128/JCM.02204-20**.

13 L. Azzi, G. Carcano, F. Gianfagna, P. Grossi, D. Gasperina, A. Genoni, M. Fasano, F. Sessa, L. Tettamanti, F. Carinci, V. Maurino, A. Rossi, A. Tagliabue and A. Baj, Saliva is a reliable tool to detect SARS-CoV-2, *J. Infect.*, 2020, **81**, 45, DOI: **10.1016/j.jinf.2020.04.005**.

14 R. Yee, T. Truong, P. Pannaraj, N. Eubanks, E. Gai, J. Jumarang, L. Turner, A. Peralta, Y. Lee, J. Dien and J. D. Bard, Saliva is a promising alternative specimen for

the detection of SARS-CoV-2 in children and adults, *Clin. Microbiol.*, 2021, **59**, 2, DOI: 10.1128/JCM.02686-20.

15 A. Teo, Y. Choudhury, I. Tan, C. Cher, S. Chew, Z. Wan, L. Cheng, L. Oon, M. Tan, K. Chan and L. Shu, Saliva is more sensitive than nasopharyngeal or nasal swabs for diagnosis of asymptomatic and mild COVID-19 infection, *Sci. Rep.*, 2021, **11**, 3134, DOI: 10.1038/s41598-021-82787-z.

16 A. Wyllie, J. Fournier, A. Casanovas-Massana, M. Campbell, M. Tokuyama, P. Vijayakumar, B. Geng, M. Muenker, A. Moore and C. Vogels, *et Al.* Saliva or Nasopharyngeal Swab Specimens for Detection of SARS-CoV-2, *N. Engl. J. Med.*, 2020, **383**, 1283, DOI: 10.1101/2020.04.16.20067835.

17 P. Moitra, M. Alafeef, K. Dighe, M. Frieman and D. Pan, Selective naked-eye detection of SARS-CoV-2 mediated by N gene targeted antisense oligonucleotide capped plasmonic nanoparticles, *ACS Nano*, 2020, **14**, 7617, DOI: 10.1021/acsnano.0c03822.

18 G. Seo, G. Lee, M. Kim, S. Baek, M. Choi, K. Ku, C. Lee, S. Jun, D. Park, H. Kim, S. Kim, J. Lee, B. Kim, E. Park and S. Kim, Rapid Detection of COVID-19 Causative Virus (SARS-CoV-2) in Human Nasopharyngeal Swab Specimens Using Field-Effect Transistor-Based Biosensor, *ACS Nano*, 2020, **14**, 5135, DOI: 10.1021/acsnano.0c02823.

19 P. Fathi-Hafshejani, N. Azam, L. Wang, M. Kuroda, M. Hamilton, S. Hasim and M. Mahjouri-Samani, Two-dimensional-material-based Field-Effect Transistor biosensor for detecting COVID-19 Virus (SARS-CoV-2), *ACS Nano*, 2021, **15**, 11461, DOI: 10.1021/acsnano.1c01188.

20 A. Stergiou, R. Canton-Vitoria, M. N. Psarrou, S. P. Economopoulos and N. Tagmatarchis, Functionalized graphene and targeted applications – Highlighting the road from chemistry to applications, *Prog. Mater. Sci.*, 2020, **114**, 100683, DOI: 10.1016/j.pmatsci.2020.100683.

21 S. Presolski and M. Pumera, Covalent functionalization of MoS_2, *Mater. Today*, 2016, **19**, 140, DOI: 10.1016/j.mattod.2015.08.019.

22 C. Stangel, E. Nikoli and N. Tagmatarchis, Transition metal dichalcogenides interfacing photoactive molecular components for managing energy conversion processes, *Adv. Energy Sustainability Res.*, 2022, **3**, 2200097, DOI: 10.1002/aesr.202200097.

23 R. Canton-Vitoria, H. B. Gobeze, V. M. Blas-Ferrando, J. Ortiz, Y. Jang, F. Fernández-Lázaro, Á. Sastre-Santos, Y. Nakanishi, H. Shinohara, F. D'Souza and N. Tagmatarchis, Excited-state charge transfer in covalently functionalized MoS_2 with a Zinc phthalocyanine donor–acceptor hybrid, *Angew. Chem.*, 2019, **131**, 5768, DOI: 10.1002/anie.201900101.

24 R. Canton-Vitoria, T. Scharl, A. Stergiou, A. Cadranel, R. Arenal, D. M. Guldi and N. Tagmatarchis, Ping-pong energy transfer in covalently linked porphyrin-MoS_2 architectures, *Angew. Chem., Int. Ed.*, 2020, **59**(1), 3976, DOI: 10.1002/anie.201914494.

25 R. Canton-Vitoria, E. Istif, J. Hernández-Ferrer, E. Urriolabeitía, A. Benito, W. Maser and N. Tagmatarchis, Integrating water-Soluble polythiophene with transition-metal dichalcogenides for managing photoinduced processes, *ACS Appl. Mater. Interfaces*, 2019, **11**, 5947, DOI: 10.1021/acsami.8b18435.

26 L. Vallan, R. Canton-Vitoria, H. B. Gobeze, Y. Jang, R. Arenal, A. M. Benito, W. K. Maser, F. D'Souza and N. Tagmatarchis, Interfacing transition metal dichalcogenides with carbon nanodots for managing photoinduced energy and charge-transfer processes, *J. Am. Chem. Soc.*, 2018, **140**, 13488, DOI: 10.1021/jacs.8b09204.

27 R. Canton-Vitoria, L. Vallan, E. Urriolabeitia, A. M. Benito, W. K. Maser and N. Tagmatarchis, Electronic interactions in illuminated carbon dot/MoS_2 ensembles and electrocatalytic activity towards hydrogen evolution, *Chem. – Eur. J.*, 2018, **24**, 10468, DOI: 10.1002/chem.201801425.

28 R. Canton-Vitoria, Y. Sayed-Ahmad-Baraza, M. Pelaez-Fernandez, R. Arenal, C. Bittencourt, P. C. Ewels and N. Tagmatarchis, Functionalization of MoS_2 with 1,2-dithiolanes: toward donor-acceptor nanohybrids for energy conversion, *npj 2D Mater. Appl.*, 2017, **1**, 1, DOI: 10.1038/s41699-017-0012-8.

29 I. K. Sideri, Y. Jang, J. Garcés-Garcés, A. Sastre-Santos, R. Canton-Vitoria, R. Kitaura, F. Fernández-Lázaro, F. D'Souza and N. Tagmatarchis, Unveiling the Photoinduced Electron-Donating Character of MoS_2 in Covalently Linked Hybrids Featuring Perylenediimide, *Angew. Chem., Int. Ed.*, 2021, **60**, 9120, DOI: 10.1002/anie.202016249.

30 R. Canton-Vitoria, Y. Sayed-Ahmad-Baraza, R. Arenal, C. P. Ewels and N. Tagmatarchis, Pyrene-functionalized tungsten disulfide as stable resistive photosensor, *Mater. Adv.*, 2020, **10**, 363, DOI: 10.1039/d0ma00429d.

31 R. Canton-Vitoria, S. Nufer, X. Che, Y. Sayed-Ahmad-Baraza, R. Arenal, C. Bittencourt, A. Brunton, B. A. Dalton, P. C. Ewels and N. Tagmatarchis, Pyrene coating transition metal disulfides as protection from photooxidation and Environmental Aging, *Nanomaterials*, 2020, **10**(2), 363, DOI: 10.3390/nano10020363.

32 P. M. Minadakis, R. Canton-Vitoria, C. Stangel, E. Klontzas, R. Arenal, J. Hernandez-Ferrer, M. Benito, A. K, W. Maser and N. Tagmaterchis, Tungsten disulfide interfacing nickel-porphyrin for photo-enhanced electrocatalytic water oxidation, *ChemSusChem*, 2023, DOI: 10.1002/cssc.202202322, In press.

33 L. Piccoli, Y. Park, M. Tortorici, N. Czudnochowski, A. Walls, M. Beltramello, C. Silacci-Fregni, D. Pinto, L. Rosen, J. Bowen, O. J. Acton, S. Jaconi, B. Guarino, A. Minola, F. Zatta, N. Sprugasci, J. Bassi, A. Peter and D. Veesler, Mapping neutralizing and immunodominant sites on the SARS-CoV-2 spike receptor-binding domain by structure-guided high-resolution serology, *Cell*, 2020, **183**, 1024, DOI: 10.1016/j.cell.2020.09.037. PDB ID 7JX3 _B.

34 F. Wu, S. Zhao, B. Yu, Y. Chen, W. Wang, Z. Song, Y. Hu, Z. Tao, J. Tian, Y. Pei, M.-L. Yuan, Y.-L. Zhang, F.-H. Dai, Y. Liu, Q.-M. Wang, J.-J. Zheng, L. Xu, E. C. Holmes and Y.-Z. Zhang, A new coronavirus associated with human res-

piratory disease in China, *Nature*, 2020, **579**, 265, DOI: 10.1038/s41586-020-2008-3. PDB ID: 7fG7.

35 R. Canton-Vitoria, T. Hotta, Z. Liu, T. Inoue and R. Kitaura, Stabilization of metallic phases through formation of metallic/semiconducting lateral heterostructures, *J. Chem. Phys.*, 2020, **153**, 084702.

36 R. Canton-Vitoria, T. Hotta, M. Xue, S. Zhang and R. Kitaura, Synthesis and characterization of transition metal dichalcogenides nanoribbons based on a controllable O_2 etching, *JACS Au*, 2022, DOI: 10.1021/jacsau.2c00536, In press.

37 T. Starr, N. Czudnochowski, Z. Liu, F. Zatta, Y. Park, A. Addetia, D. Pinto, M. Beltramello, P. Hernandez, A. J. Greaney, R. Marzi, W. G. Glass, I. Zhang, A. S. Dingens, J. E. Bowen, M. A. Tortorici, A. C. Walls, J. A. Wojcechowsky, A. D. Marco, L. E. Rosen, J. Zhou, M. Montiel-Ruiz, H. Kaiser, J. R. Dillen, H. Tucker, J. Bassi, C. Silicci-Fregni, M. P. Housley, J. D. Lulio, G. Lombardo, M. Agostini, N. Sprugasci, K. Culap, S. Jaconi, M. Meury, E. Dellota, R. Adbelnabi, S.-Y. C. Foo, E. Cameroni, S. Stumpf, T. I. Croll, J. C. Nix, C. Havenar-Daughton, L. Piccoli, F. Benigni, J. Neyts, A. Telenti, F. A. Lempp, M. S. Pizzuto, J. D. Chodera, C. M. Herbner, H. W. Virgin, S. P. J. Whelan, D. Veesler, D. Corti, J. D. Bloom and G. Snell, SARS-CoV-2 RBD antibodies that maximize breadth and resistance to escape, *Nature*, 2021, **597**, 97, DOI: 10.1038/s41586-021-03807-6. PDB ID 7R6X_C.

38 A. de Moraes and L. Kubota, Recent Trends in Field-Effect Transistors-Based Immunosensors, *Chemosensors*, 2016, **4**, 20, DOI: 10.3390/chemosensors4040020.

39 S. N. Kajale, S. Yadav, Y. Cai, B. Joy and D. Sarkar, 2D material based field effect transistors and nanoelectromechanical systems for sensing applications, *iScience*, 2021, **24**, 103513, DOI: 10.1016/j.isci.2021.103513.

40 P. Shen, C. Su, Y. Lin, A. Chou, C. Cheng, J. Park, M. Chiu, A. Lu, H. Tang, M. Tavakoli, G. Piter, X. Ji, Z. Cai, N. Mao, J. Wang, V. Tung, J. Bokor, A. Zettl, C. Wu, T. Palacios, L.-J. Li and J. Kong, Ultralow contact resistance between semimetal and monolayer semiconductors, *Nature*, 2021, **593**, 211–217, DOI: 10.1038/s41586-021-03472-9.

41 D. Perivoliotis, Y. Sato, K. Suenaga and N. Tagmatarchis, Covalently functionalized layered MoS_2 supported Pd nanoparticles as highly active oxygen reduction electrocatalysts, *Nanoscale*, 2020, **12**, 18278, DOI: 10.1039/D0NR04446F.

42 G. Tsaltas and C. H. j. Ford, Cell Membrane Antigen-Antibody Complex Dissociation by the Widely Used Glycine-Hcl Method: An Unreliable Procedure for Studying Antibody Internalization, *Immunol. Invest.*, 1993, **12**, 1, DOI: 10.3109/08820139309066189.

43 E. Andreano, E. Nicastri, I. Paciello, P. Pileri, N. Manganaro, G. Piccini, A. Maneti, E. Pantano, A. Kabanova, M. Troisi, F. Vacca, D. Cardamone, C. D. Canti, J. L. Torres, G. Ozorowski, L. Benincasa, H. Jang, C. D. Genova, L. Depau, J. brunetti, C. Agrati, M. R. Capobianchi, C. Castilletti, A. Emiliozzi, M. Fabbiani, F. Montomoli, L. Bracci, G. Sautto, T. M. Ross, E. Montomoli, N. Temperton, A. B. Ward, C. Sala, G. Ippolito and R. Rappuoli, Extremely potent human monoclonal antibodies from COVID-19 convalescent patients, *Cell*, 2021, **184**, 1821, DOI: 10.1016/j.cell.2021.02.035.

44 D. Wijesuriya, K. Breslin, G. Anderson, L. Shriver-Lake and F. S. Ligler, Regeneration of immobilized antibodies on fiber optic probes, *Biosens. Bioelectron.*, 1994, **9**, 585, DOI: 10.1016/0956-5663(94)80051-0.

45 A. Kausaite-Minkstimiene, A. Popov and A. Ramanaviciene, Surface Plasmon Resonance Immunosensor with Antibody-Functionalized Magnetoplasmonic Nanoparticles for Ultrasensitive Quantification of the CD5 Biomarker, *ACS Appl. Mater. Interfaces*, 2022, **14**, 20720, DOI: 10.1021/acsami.2c02936.

46 Y. M. Bar-On, A. Flamholz, R. Phillips and R. Milo, SARS-CoV-2 (COVID-19) by the numbers, *eLife*, 2020, **9**, e57309, DOI: 10.1073/pnas.2024815118.

47 V. Thao, B. Giang and T. Thu, Free-standing polypyrrole/polyaniline composite film fabricated by interfacial polymerization at the vapor/liquid interface for enhanced hexavalent chromium adsorption, *RSC Adv.*, 2019, **9**, 5445, DOI: 10.1039/C8RA10478F.

48 M. Zamzami, G. Rabbani, A. Ahmad, A. Basalah, W. Al-Sabban, S. N. Ahn and H. Choudhry, Carbon nanotube field-effect transistor (CNT-FET)-based biosensor for rapid detection of SARS-CoV-2 (COVID-19) surface spike protein S1, *Bioelectrochemistry*, 2022, **143**, 107982, DOI: 10.1016/j.bioelechem.2021.107982.

49 R. Canton-Vitoria, C. Stangel and N. Tagmatarchis, Electrostatic Association of Ammonium-Functionalized Layered-Transition-Metal Dichalcogenides with an Anionic Porphyrin, *ACS Appl. Mater. Interfaces*, 2018, **10**, 23476, DOI: 10.1021/acsami.8b08272.

50 Y. Zhu, D. Yu, Y. Han, H. Yan, H. Chong, L. Ren, J. Wang, T. Li and Y. He, Cross-reactive neutralization of SARS-CoV-2 by serum antibodies from recovered SARS patients and immunized animals, *Sci. Adv.*, 2020, **6**, 45, DOI: 10.1126/sciadv.abc9999.

51 A. Stergiou, C. Stangel, R. Canton-Vitoria, R. Kitaura and N. Tagmatarchis, An ion-selective crown ether covalently grafted onto chemically exfoliated MoS_2 as a biological fluid sensor, *Nanoscale*, 2021, **13**, 8948, DOI: 10.1039/D1NR00404B.

52 A. Wasfi, F. Awwad, N. Qamhieh, B. A. Murshidi, R. A. Palakkott and G. J. Gelovani, Real-time COVID-19 detection via graphite oxide-based field-effect transistor biosensors decorated with Pt/Pd nanoparticles, *Sci. Rep.*, 2022, **12**, 18155, DOI: 10.1038/s41598-022-22249-2.

53 G. Li, A. Wang, Y. Chen, Y. Sun, Y. Du, X. Wang, P. Ding, R. Jia, Y. Wang and G. Zhang, Development of a colloidal gold-based immunochromatographic strip for rapid detection of severe acute respiratory syndrome coronavirus 2 Spike Protein, *Front. Immunol.*, 2021, **12**, 560, DOI: 10.3389/fimmu.2021.635677.

54 L. A. Ardekani and P. W. Thulstrup, Gold Nanoparticle-Mediated Lateral Flow Assays for Detection of Host Antibodies and COVID-19 Proteins, *Nanomaterials*, 2022, **12**, 1456, DOI: **10.3390/nano12091456**.

55 L. F. d. Lima, A. L. Ferreira, M. D. T. Torres, W. R. de Araujo and C. de la Fuente-Nunez, Minute-scale detection of SARS-CoV-2 using a low-cost biosensor composed of pencil graphite electrodes, *Proc. Natl. Acad. Sci. U. S. A.*, 2021, **118**(30), e2106724118, DOI: **10.1073/pnas.2106724118**.